Innovative Food Science and Emerging Technologies 105 (2025) 104175

Contents lists available at ScienceDirect

Innovative Food Science and Emerging Technologies

journal homepage: www.elsevier.com/locate/ifset

Solid-state microwave phase control for improved heating patterns in single-mode cavities

Xu Zhou [a], Zhongwei Tang [b], Patrick D. Pedrow [c], Juming Tang [a,*]

[a] Department of Industrial & Systems Engineering, University of Washington, Seattle, WA 98195, USA
[b] Department of Biological Systems Engineering, Washington State University, Pullman, WA 99164, USA
[c] School of Electrical Engineering and Computer Science, Washington State University, Pullman, WA 99164, USA

ARTICLE INFO

Keywords:
Phase
Solid-state microwave
Single-mode
Heating pattern
Computer simulation

ABSTRACT

Phase control is a unique feature of solid-state microwave generators. This study investigated how solid-state phase affected microwave fields and heating patterns of foods in a 915 MHz single-mode cavity of Microwave-Assisted Pasteurization System (MAPS). A 3D computer simulation model was developed and experimentally validated using a chemical marker method. Results showed that adjusting the phase differences between the top and bottom microwave entry ports shifted electric fields patterns and moved hot and cold zones vertically along the depth of food packages. Simulations also demonstrated that phase control can align high microwave energy zones with the central layers of food packages of varying thicknesses. This would otherwise require physical conveyor adjustments in commercial microwave systems. The study provides the first experimental validation of solid-state phase control in a 915 MHz single-mode cavity and establishes a modeling framework for dynamic phase control in industrial microwave processing.

1. Introduction

Microwave heating is widely used in domestic kitchens, but broader applications in the food industry have been hindered by the limitations of traditional microwave generators, known as magnetrons. Developed during World War II, magnetrons are still the main power source in commercial microwave systems (Atuonwu & Tassou, 2019). Their disadvantages include short lifespan, high operating voltages, and the inability to precisely control microwave frequency and phase (Atuonwu & Tassou, 2018; Werner, 2020). These limitations arise from the fundamental operating mechanism of magnetrons, in which free electrons emitted from heated filaments interact with resonant cavities under a magnetic field, producing sustained oscillations that generate microwaves (Buffler, 1993; Metaxas & Meredith, 1993). The interaction is inherently unstable, causing variations in electron bunching and cavity oscillations, which in turn cause random phase outputs and unstable peak frequencies (Collins, 1948; Zhou et al., 2023).

The peak frequency of microwaves from magnetrons varies with temperature, input power, load impedance, and component aging (Collins, 1948; Resurreccion et al., 2015; Zhou, Pedrow, et al., 2023, Zhou, Tang, Pedrow, Sablani, & Tang, 2023). Previous studies have shown that such variations can negatively affect heating performance of microwave ovens (Luan, Wang, Tang, & Jain, 2017; Zhou, Pedrow, et al., 2023). In contrast, solid-state generators offer stable peak frequency and precise frequency control, which improve microwave heating uniformity and energy efficiency (Yang & Chen, 2024; Zhou, Pedrow, et al., 2023; Zhou, Tang, et al., 2023).

On the other hand, it is difficult, or almost impossible, to control the relative phases of microwaves from multiple magnetrons, because their peak frequencies are unstable and cannot be synchronized. A phase difference can be introduced by splitting the output from a single magnetron into two or more waveguides having different waveguide lengths or using sliding shorts (Bows, Patrick, Janes, & Dibben, 1999; Luan, Tang, Pedrow, Liu, & Tang, 2016), but this method is not suitable for precise and dynamic phase control.

Recent advances in solid-state microwave generators offer a promising solution to long-standing challenges, such as non-uniform heating caused by standing waves in cavities. Solid-state systems use semiconductor-based amplifiers that enable precise control of phase and frequency (Atuonwu & Tassou, 2018; Werner, 2020; Zhou, Pedrow, et al., 2023). Multiple solid-state power sources can be synchronized electronically, allowing precise control of phase differences between microwave inputs. The phase differences influence electric field distributions and temperature patterns within food products. Studies using

* Corresponding author.
E-mail address: jutang88@uw.edu (J. Tang).

https://doi.org/10.1016/j.ifset.2025.104175
Received 3 May 2025; Received in revised form 16 August 2025; Accepted 17 August 2025
Available online 18 August 2025

2450 MHz multi-mode cavities (e.g., domestic microwave ovens) showed that phase adjustment or phase sweeping with solid-state generators can improve microwave heating uniformity (Ahn, Jeong, & Lee, 2023; Ghimire & Chen, 2025; Li et al., 2025; Verma et al., 2024). For example, Li et al. (2025) demonstrated a solid-state microwave phase optimization method that used computer simulation models and real-time volumetric temperature feedback to improve heating uniformity.

However, there is a lack of systematic research on phase control in industrial 915 MHz single-mode cavities. The 915 MHz frequency is preferred for industry use due to deeper penetration in foods. Single-mode cavities provide predictable electromagnetic fields, making them particularly suitable for thermal processing for pathogen control (Tang, 2015). Researchers at Washington State University (WSU) developed pilot-scale Microwave-Assisted Thermal Sterilization (MATS) system and Microwave-Assisted Pasteurization System (MAPS) that use specially designed 915 MHz single-mode cavities (Tang, 2015; Tang, Hong, Inanoglu, & Liu, 2018). These systems were used to collect engineering data for regulatory filings and to guide industrial scale-up (Tang, 2015). Based on the MATS/MAPS platform, three medium-scale continuous systems (MATS-30 and MATS-45) with the capacity of processing 30–45 single-serving meals per minute have recently been deployed in commercial production by TATA in India (Ross, Sablani, & Tang, 2023; Zhou & Tang, 2024). This success has raised strong interest in broader adoption for both sterilization and pasteurization applications.

Inspite of the advantages of solid-state microwave generators, they are still rarely used in commercial microwave systems in the food industry. Understanding how phase control of solid-state generators affects microwave field distributions and heating patterns of foods in MATS/MAPS systems would facilitate industrial adoption of solid-state technology. In this study, we used a MAPS cavity powered by a 915 MHz solid-state generator to: (1) develop a computational model to analyze how phase differences influence electric fields and heating patterns, (2) experimentally validate the model using a chemical marker method, and (3) apply the validated model to demonstrate how phase control can improve heating patterns in foods.

2. Materials and methods

2.1. Solid-state-powered microwave cavity

Fig. 1 and Fig. S1 show the single-mode microwave cavity in the pilot-scale MAPS. The cavity was sandwiched between top and bottom horn-shaped applicators, each equipped with a microwave entry port (Chen, Tang, & Liu, 2007; Tang, Liu, Pathak, & Eves, 2006). Each port was connected via waveguides to a 3 kW, 915 MHz Gallium Nitride (GAN) solid-state power head (RFHIC, South Korea). The two solid-state power heads were electronically synchronized, which can allow a controlled phase between 0° and 360°. Detailed cavity dimensions are provided in the Supplementary Material (Fig. S2). During operation, food trays were transported through the cavity by metal carriers (Jain, Tang, Liu, Tang, & Pedrow, 2018; Tang & Liu, 2020). To reduce edge heating and improve impedance matching, the cavity was filled with reverse osmosis (RO) water preheated to an elevated temperature (Gezahegn et al., 2021; Tang, 2015).

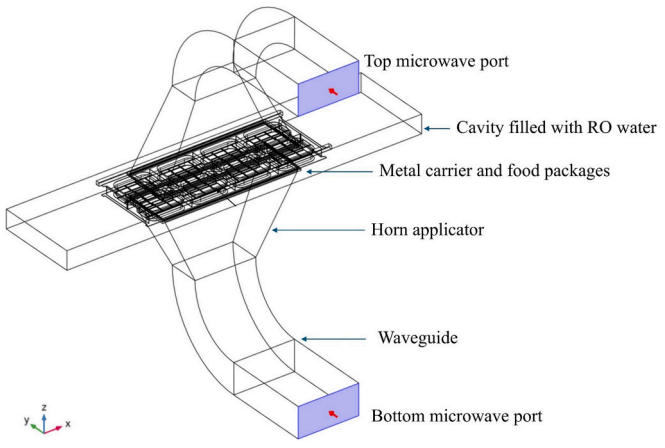

Fig. 1. Schematic of 915 MHz single-mode cavity of Microwave-Assisted Pasteurization System (MAPS), powered by two solid-state power heads connected to the top and bottom microwave ports.

2.2. Computer simulation

2.2.1. Governing equations and boundary conditions

A 3D COMSOL Multiphysics® model was developed to simulate electric field distribution and resulting temperature profiles of food materials. The test food material was made of gellan gel (Zhou, Lin, Wu, Sablani, & Tang, 2025).

Electromagnetic fields in the cavity were governed by Maxwell's equations in phasor form (Sadiku, 2018):

$$\nabla\cdot\widetilde{\mathbf{E}} = 0 \tag{1}$$

$$\nabla\cdot\widetilde{\mathbf{H}} = 0 \tag{2}$$

$$\nabla\times\widetilde{\mathbf{E}} = -j\omega\mu\widetilde{\mathbf{H}} \tag{3}$$

$$\nabla\times\widetilde{\mathbf{H}} = j\omega\widetilde{\varepsilon}\widetilde{\mathbf{E}} \tag{4}$$

where $\widetilde{\mathbf{E}}$ is the electric field phasor (V/m), $\widetilde{\mathbf{H}}$ is the magnetic field phasor (A/m), μ is the magnetic permeability (H/m), and ω is the angular frequency (rad/s).

$$\omega = 2\pi f \tag{5}$$

where f is microwave frequency (Hz).

The complex permittivity $\widetilde{\varepsilon}$ was defined as:

$$\widetilde{\varepsilon} = \varepsilon_0(\varepsilon' - j\varepsilon'') \tag{6}$$

where ε_0 is vacuum permittivity (=8.85 × 10^{-12}F/m), ε' is the relative (to air) dielectric constant, and ε'' is the relative dielectric loss factor of the food material or water. Dielectric properties of RO water at 90 °C were obtained from Gezahegn et al. (2021). The metallic cavity walls and the food carrier were assumed to be perfect electric conductors (PECs).

Assuming time-harmonic fields in a linear, isotropic, homogeneous medium, Maxwell's equations reduced to the Helmholtz equations:

$$\nabla^2\mathbf{E} + \omega^2\mu\widetilde{\varepsilon}\mathbf{E} = 0 \tag{7}$$

$$\nabla^2\mathbf{H} + \omega^2\mu\widetilde{\varepsilon}\mathbf{H} = 0 \tag{8}$$

The conversion of the electromagnetic power to heat was calculated from the time-averaged Poynting theorem (Metaxas & Meredith, 1993):

$$P_v = \frac{1}{2}\omega\varepsilon_0\varepsilon''\left|\widetilde{\mathbf{E}}\right|^2 \tag{9}$$

where P_v is the heat generation per unit volume (W/m^3), and $|\widetilde{E}|$ is the magnitude of the electric field phasor (V/m).

Heat transfer inside the solid food samples was:

$$\rho C_p\frac{\partial T}{\partial t} = \nabla\cdot(k\nabla T) + P_v \tag{10}$$

where ρ is the material density (kg/m^3), C_p is the specific heat (J/(kg°C)), and k is the thermal conductivity (W/(m°C)) of the food matrix. T is temperature (°C) and t is time (s).

Convective heat transfer at the food tray surface was:

$$q'' = h(T_{water} - T_s) \quad (11)$$

where q'' is surface heat flux (W/m^2), T_{water} is water temperature (maintained at 90 ± 0.5 °C by the heat exchanger and circulating system), Ts is food surface temperature (°C), and h is the convective heat transfer coefficient (h = 190 W/(m^2•°C), Jain et al. (2018)).

2.2.2. Gellan gel model food

The gellan gel samples contained 0.5% salt and were prepared following Zhou et al. (2025): 1.0% (*w/v*) gellan gum powder (KELCOGEL, CP Kelco, GA), 0.2% (w/v) titanium dioxide (Lorann Oils, MI), and 0.5% (w/v) sodium chloride were mixed with 100 mL of distilled and deionized water. The mixture was then stirred and heated on a hot plate close to the boiling point. The mixture was held for 5 min to fully hydrate the gellan gum. Afterward, 0.1% (w/v) calcium chloride ($CaCl_2{\cdot}2H_2O$, Avantor Performance Materials, PA) was added, and the solution was allowed to cool naturally. When the temperature decreased to 60 °C, chemical marker precursors—4% (w/v) D-fructose and 2% (w/v) L-lysine (Thermo Fisher Scientific, Nazareth, PA, USA)—were added and mixed thoroughly. The prepared gellan solution was then poured into plastic trays (138 mm × 94 mm × 20 mm) and cooled further to form solid gel slabs as model samples. The trays with the samples were vacuum-sealed (99% vacuum, 10 mbar absolute pressure).

The dielectric properties of the gellan gel samples were measured using a network analyzer (8752C, Hewlett-Packard, CA, USA) with an open-ended coaxial probe (Gezahegn et al., 2021). The system was calibrated using air, short, and deionized water at 25 °C (Zhou et al., 2024). An oil bath was used to heat the samples from 25 to 95 °C. Table 1 shows the temperature-dependent dielectric properties measured at 915 MHz. Thermal properties, including specific heat capacity, density, and thermal conductivity, were obtained from Zhou et al. (2024).

2.2.3. Simulation setup

A physics-controlled tetrahedral mesh was used to discretize the cavity, waveguides, and food domains. Sensitivity tests for mesh refinement were conducted using COMSOL normal, fine, finer, and extra fine settings. Convergence was reached when further refinement changed the average electric field by less than 2%, and the finer mesh was chosen. The mesh contained approximately 3.5 million elements, and solver residuals met COMSOL default tolerances of $<10^{-3}$. For transient heat transfer simulations, time steps were reduced from 0.20 to 0.05 min for a total microwave heating time of 2.0 min. A 0.10 min step was chosen for the best balance between simulation accuracy and computational time. A two-way coupled model was used: the electromagnetic field was solved in the frequency domain (Eqs. 7, 8), the resulting volumetric heat generation was calculated (Eq. 9) and applied to the heat transfer model (Eq. 10), and the temperature-dependent dielectric properties (Eq. 6) were then updated for the next simulation cycle. Simulations were performed on a high-performance workstation (XPS 8960, Intel Core i9-13900K, 24 cores, 64 GB RAM, Windows 11 Enterprise, Dell Inc.). The average computational time for each test run was about 3 h.

Table 1
Dielectric properties of gellan gel model food (0.5% salt) measured at 915 MHz* (n = 3).

Temperature (°C)	Relative dielectric constant	Relative loss factor
25	74.2 ± 0.3	27.1 ± 0.4
50	67.5 ± 1.3	30.1 ± 0.8
65	64.4 ± 1.2	33.1 ± 3.2
80	65.6 ± 4.8	41.5 ± 1.0
95	62.8 ± 1.5	46.1 ± 4.1

* Dielectric properties are assumed to be the same at 902 MHz (used in simulations) and 915 MHz (measured by the network analyzer).

2.3. Experimental validation

Gellan gel samples in sealed trays were preheated in 51 °C water in MAPS for 20 min to equilibrate internal temperature (Zhou et al., 2025). The carrier with the sample trays was then moved to the microwave cavity (filled with circulating RO water at 90 °C) and held stationary for 2 min. Microwaves from the two solid-state power heads were supplied to the cavity (Fig. 1). Each solid-state power head had a built-in detector to monitor forward and reflect power in real time. A frequency of 902 MHz (within the 902–928 MHz range) was selected based on total reflected power measurements from the two detectors, which showed minimal power reflection for the tested sample. After microwave heating, the food carrier was moved at 1.63 m/min (64 inch/min) to a cooling section and cooled in 20 °C water for 20 min.

Phase differences of 0°, 90°, 180°, or 270° were applied between the two ports. Heating patterns in the samples were visualized by measuring CIE L^* color values (Zhou et al., 2025). Prior to the measurement, samples were removed from the trays, and cut horizontally to show the middle layers or cut vertically for cross sections. Images were taken using a Nikon camera and calibrated with a QP card (Zhou, Lin, Wu, Sablani and Tang, 2025).

3. Results and discussions

3.1. Experimental validation of simulation model

Fig. 2 compares experimental and simulated heating patterns of the gellan gel samples after being heated in the the microwave cavity with a 180° phase difference. The images show the heating patterns in horizontal and vertical planes. In the horizontal middle layer, both experiment and simulation identified a central hot spot and cold spots near the edges. Similarly, vertical cross-sections from both simulation and experiment showed a hot spot in the central zone and a cold spot in the left-central region of the sample. Fig. 3 compares experimental and simulated results along the sample thickness for different phase differences (0°, 90°, 180°, and 270°). Overall, the experimental and simulated results agreed well in the locations of hot and cold spots. There were some discrepancies, mainly because the chemical marker method captured the accumulated thermal effects over the entire process, whereas simulations showed instantaneous temperature distributions of microwave heating. Nonetheless, the locations of hot and cold spots—which are critical for thermal processing—were well aligned between the experiment and simulation, which validated our computer simulation models.

3.2. Phase control to change vertical heating patterns

Fig. 3 also shows that phase control effectively shifted the vertical locations of hot and cold spots (i.e., along the food thickness). This demonstrated the potential to improve vertical heating uniformity, which is more challenging to achieve in MAPS and MATS systems than horizontal heating uniformity. Horizontal heating uniformity (in the x-y plane, Fig. 1) can be improved by moving food carriers or optimizing the carrier design (Jain et al., 2018; Tang & Liu, 2020). In this study, the optimized carrier design (Tang & Liu, 2020) was used. The horizontal movement (i.e., along x-direction in Fig. 1) during continuous processing would not influence the vertical (z direction) microwave field distribution, so a separate method is needed to improve vertical heating patterns.

Luan et al. (2016) theoretically showed that adjusting phase differences could vertically shift microwave hot and cold zones in MATS cavities. Experimental validation was not possible at the time because the magnetron systems do not allow precise control of phase differences. The present study provides the first experimental validation of this prediction using a solid-state microwave generator. It is worth mentioning that there was one difference between our results and Luan

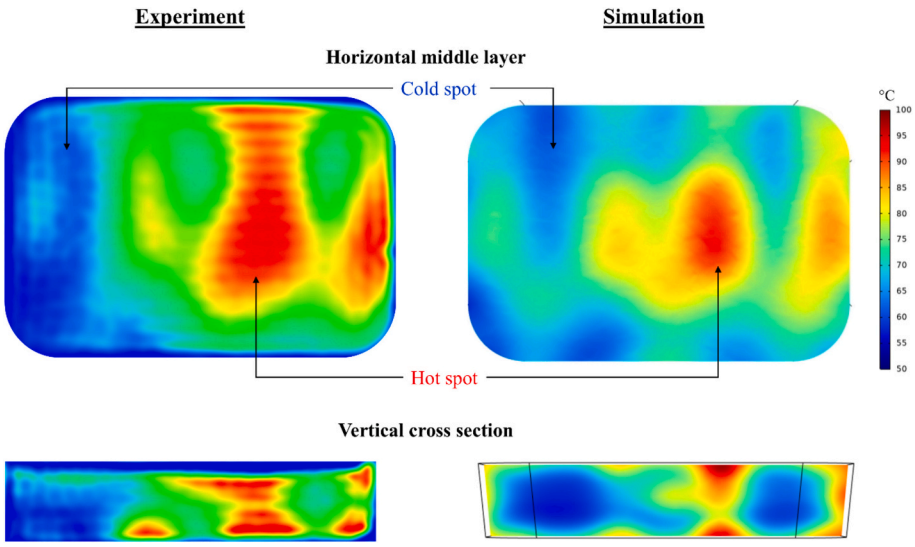

Fig. 2. Experimental heating patterns and simulated temperature distributions in the gellan gel model food at the phase difference of 180°. (top) Horizontal middle layer and (bottom) vertical cross-section views.

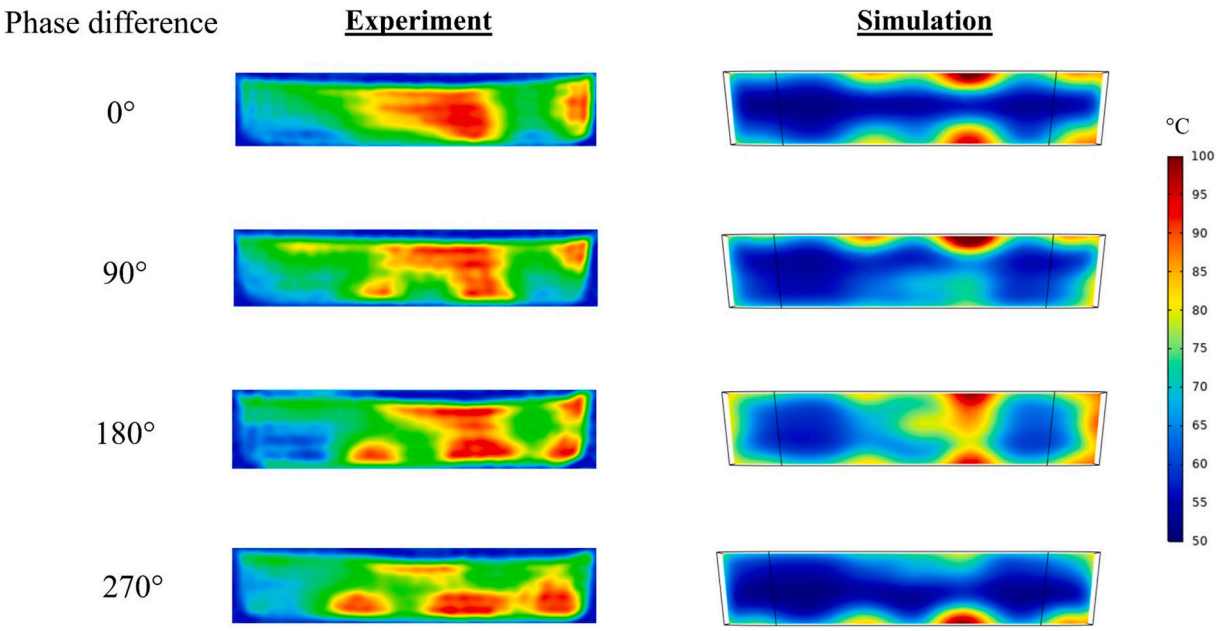

Fig. 3. Experimental heating patterns and simulated temperature distributions along the thickness of gellan gel model food under different phase differences (0°, 90°, 180°, 270°).

et al. (2016). In the simulation presented in Luan et al. (2016), a 0° phase difference produced a central hot spot, whereas in this study, a 180° phase difference yielded a similar pattern. This difference was caused by the 22 cm WR975 waveguide used in the Luan et al. (2016) simulation, which introduced a 180° phase shift. This can be explained as follows:

When microwaves propagate in a waveguide, the wavelength in a waveguide λ_g is calculated by (Sadiku, 2018):

$$\lambda_g = \frac{\lambda_0}{\sqrt{1-(\lambda_c/\lambda_0)^2}} \tag{12}$$

where λ_0 is the free-space wavelength (m), and λ_c is the cutoff wavelength (m).

For 915 MHz microwaves,

$$\lambda_0 = \frac{c}{f} = \frac{3\times10^8 \text{m/s}}{9.15\times10^8 \text{Hz}} \approx 0.328\text{m} \tag{13}$$

For the rectangular WR975 waveguide in TE_{10} mode,

$$\lambda_c = 2a \tag{14}$$

where a is the width of the wider wall of the waveguide. For the WR975 waveguide, $a = 0.248$ m, so $\lambda_c = 2 \times 0.248$ m $= 0.496$ m.

Substituting Eqs. (13) and (14) into Eq. (12):

$$\lambda_g = \frac{0.328}{\sqrt{1-\left(\frac{0.328}{0.496}\right)^2}} \approx 0.44\text{m} = 44\text{cm} \tag{15}$$

The phase shift due to the 22 cm waveguide used in Luan et al.

(2016) is:

$$\Delta\varphi = \frac{\Delta x}{\lambda_g} \bullet 360^{\circ} = \frac{22}{44} \bullet 360^{\circ} = 180^{\circ} \quad (16)$$

In our solid-state system as shown in Fig. 1, phase was controlled electronically, and no extra waveguide for the phase adjustment was used. Thus, the phase difference at the cavity ports directly matched the set value of the solid-state generator.

3.3. Effect of phase difference on electric fields

The validated simulation model was used to visualize electric field (*E*-field) distribution in the microwave cavities which are nearly impossible to measure experimentally. Fig. 4 (front view) and Fig. 5 (side view) show simulated E-field patterns, with and without food packages, for phase differences of 0°, 90°, 180°, and 270°.

Without food, clear standing wave patterns were observed along the vertical axis, caused by constructive and destructive interference between microwaves entering from the top and bottom ports. Similar results were reported in single-mode MATS system (Hong, Stanley, Tang, Bui, & Ghandi, 2021; Luan et al., 2016). The standing waves created alternating nodes (low E-field strength) and anti-nodes (high E-field strength) at predictable vertical positions. At 0° phase difference, a central node with minimal microwave energy was present, whereas a 180° difference produced a central anti-node with maximum intensity. At 90° and 270°, the interference pattern shifted without clear nodes or anti-nodes at the central plane. The distance between adjacent nodes or anti-nodes depended on the microwave wavelength within the dielectric medium, as discussed in Tang (2015) and Luan et al. (2016).

When food and carrier were present, the E-field distribution was distorted, but the main observation remained: phase control effectively shifted the vertical position of high- and low-field regions. For example, at 180°, a high E-field intensity aligned with the food center, confirming phase control as a practical tool to manipulate E-field patterns.

3.4. Phase control to align hot zone with food center

In MATS and MAPS, food packages travel through microwave cavities while immersed in circulating hot water (Tang, 2015; Tang et al., 2018). The hot water provides convective heating at the surfaces, making the geometric center of the food the coldest region. In single-mode MATS/MAPS cavities, standing waves create microwave "hot" and "cold" zones along the vertical axis, as discussed above. For optimal heating, the food center (the coldest zone from hot water) should align with one of the microwave hot zones. In commercial systems, this alignment is usually achieved by adjusting the conveyor height to reposition food packages or metal carriers vertically. However, this approach is impractical for products of varying thicknesses, especially when frequent adjustments are required. We hypothesized that solid-state microwave phase control could offer an alternative by electronically shifting the vertical position of microwave hot zones without altering conveyor height.

To test this idea, we used the validated simulation model to evaluate phase control for food package thicknesses of 20, 26, and 30 mm which represents the typical thicknesses of commercial single-serving meal trays for MATS/MAPS processing. A series of phase differences, at 5° intervals (0°, 5°, 10°, 15°, 20°, etc.), was first tested in the simulation. The results (not shown) indicated that small changes in phase—less than 30°—had minimal effects on the E-field distributions. For practical comparison, phase settings of 0°, 45°, 90°, and 135° were selected and presented. Fig. 6 shows how phase adjustment shifted hot zones. For example, a 45° phase difference positioned the hot spot near the center of 20 mm thick food packages. On the other hand, a 135° difference centered the hot zone within 30 mm packages. These results validate our idea and confirm that phase control can effectively adjust vertical heating patterns to accommodate different package thicknesses without physical conveyor adjustments.

4. Conclusion

This study provides the first experimental validation of phase control in a 915 MHz solid-state single-mode MAPS cavity and demonstrates its

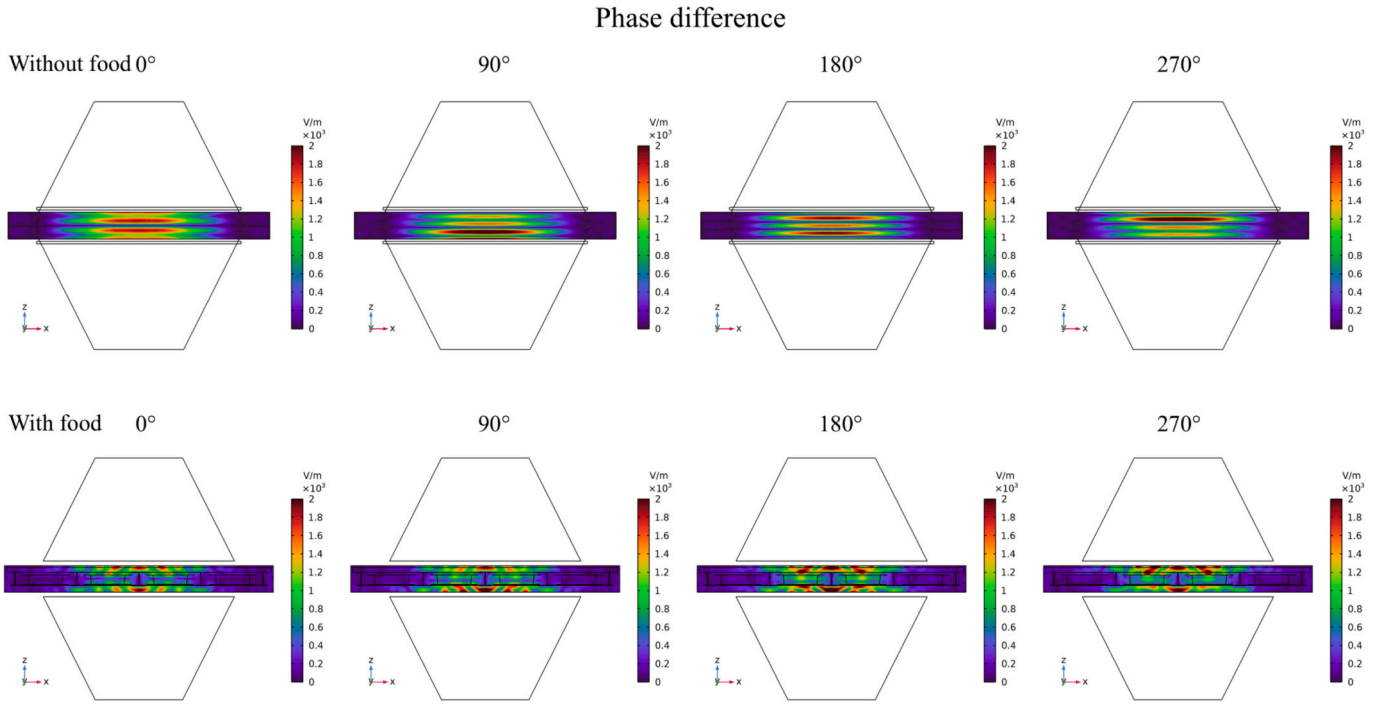

Fig. 4. Simulated electric field distributions (front view, x-z in Fig. 1) in the cavity filled with RO water under four phase differences (0°, 90°, 180°, 270°) between the top and bottom ports. Results are shown for both unloaded (without food) and loaded (with food) cavity conditions.

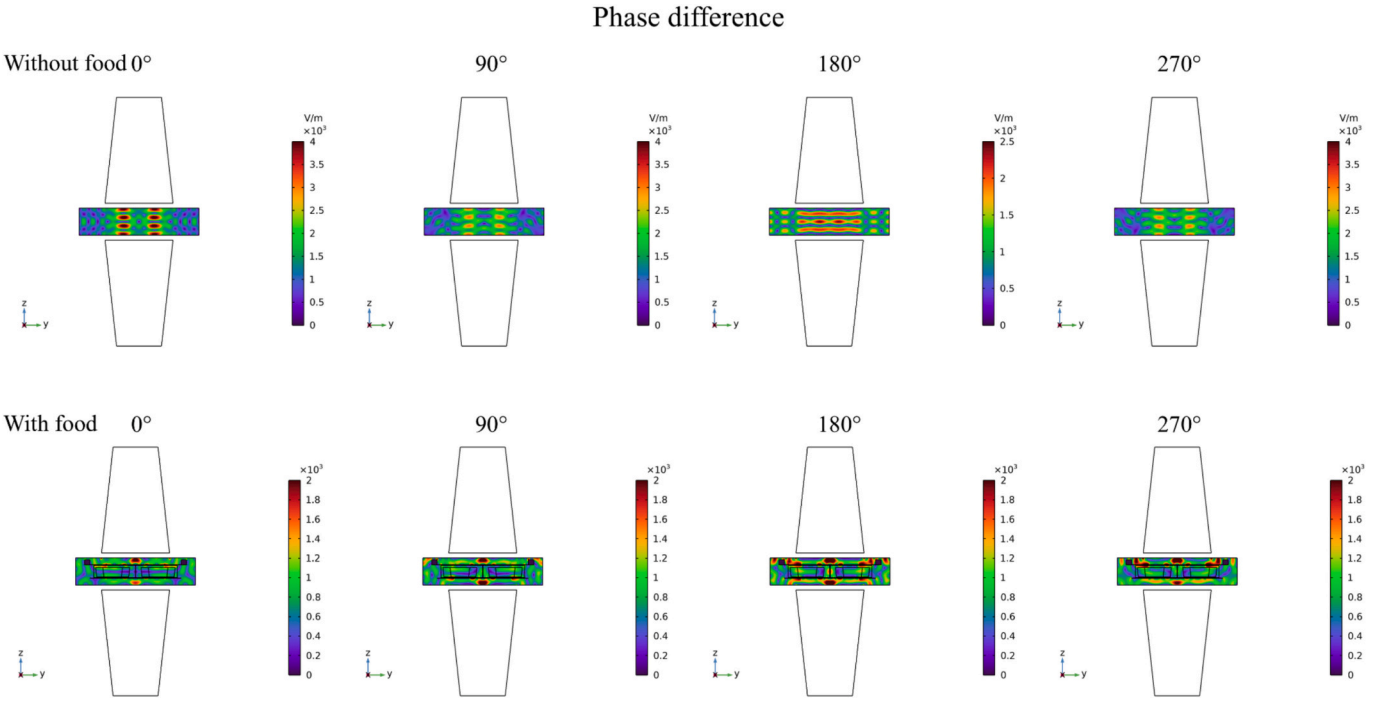

Fig. 5. Simulated electric field distributions (side view, y-z in Fig. 1) in the cavity filled with RO water under four phase differences (0°, 90°, 180°, 270°) between the top and bottom ports. Results are shown for both unloaded (without food) and loaded (with food) cavity conditions.

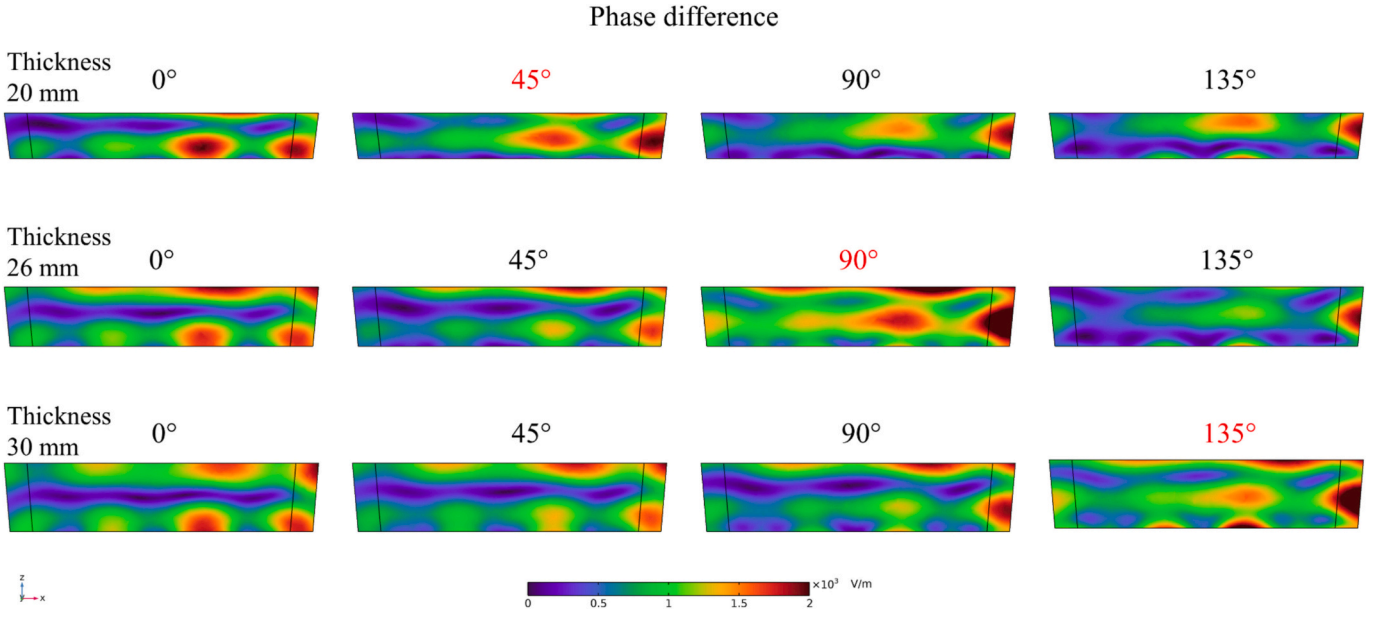

Fig. 6. Simulated electric field distributions (V/m) in food samples of different thicknesses (20, 26, and 30 mm) under selected phase differences (0°, 45°, 90°, 135°). Phase values marked in red indicate that the hot zone aligns with food center layer. (For interpretation of the references to color in this figure legend, the reader is referred to the web version of this article.)

ability to manipulate heating patterns within food packages. A 3D computer simulation model, validated using a chemical marker method, showed that adjusting the phase difference between top and bottom microwave inputs can vertically shift microwave hot and cold zones (i.e., along the depth of food packages). This allows the microwave hot spot to align with the geometric center of the package. This capability is particularly important in MATS/MAPS systems, where the food center is usually the coldest region during processing due to surrounding hot water heating. Phase control provides a practical, non-mechanical way to improve vertical heating patterns for products of different thicknesses, which cannot be achieved with conventional magnetron-based systems.

Future research will test real food samples to quantify improvements in temperature uniformity and quality when applying phase control. Computer simulations can be run with different food products with different dielectric properties, multi-component arrangements, geometries, dimensions, and shapes (Li et al., 2025), to build a phase-heating pattern database. Ideally, selected phase settings should produce

complementary heating patterns, that is, cold spots in one phase setting become hot spots in another to maximize overall microwave heating uniformity. The database could enable intelligent control of solid-state generators for different food products. In multi-cavity industrial microwave systems, when dynamic control is not preferred, each solid-state-powered cavity could be assigned a different fixed phase difference.

CRediT authorship contribution statement

Xu Zhou: Writing – original draft, Methodology, Investigation, Conceptualization. **Zhongwei Tang:** Writing – review & editing, Investigation. **Patrick D. Pedrow:** Writing – review & editing. **Juming Tang:** Conceptualization, Writing – review & editing, Supervision, Project administration.

Declaration of competing interest

The named authors have no conflict of interest.

Acknowledgement

This work was supported by USDA National Institute of Food and Agriculture (NIFA), Agriculture and Food Research Initiative (AFRI) Grant No. 2023-67017-39831, and the start-up fund from University of Washington.

Appendix A. Supplementary data

Supplementary data to this article can be found online at https://doi.org/10.1016/j.ifset.2025.104175.

Data availability

Data will be made available on request.

References

Ahn, S. H., Jeong, C. H., & Lee, W. S. (2023). 0.5 kWatt 2.45 GHz GaN-based microwave heating system design with active phase control. *Microwave and Optical Technology Letters, 65*(8), 2158–2164.

Atuonwu, J. C., & Tassou, S. A. (2018). Quality assurance in microwave food processing and the enabling potentials of solid-state power generators: a review. *Journal of Food Engineering, 234*, 1–15.

Atuonwu, J. C., & Tassou, S. A. (2019). Energy issues in microwave food processing: A review of developments and the enabling potentials of solid-state power delivery. *Critical Reviews in Food Science and Nutrition, 59*(9), 1392–1407.

Bows, J. R., Patrick, M. L., Janes, R., & Dibben, D. C. (1999). Microwave phase control heating. *International Journal of Food Science and Technology, 34*(4), 295–304.

Buffler, R. C. (1993). *Microwave [c]ooking and [P]rocessing.* Springer US, New York: Van Nostrand Reinhold.

Chen, H., Tang, J. M., & Liu, F. (2007). Coupled simulation of an electromagnetic heating process using the finite difference time domain method. *Journal of Microwave Power and Electromagnetic Energy, 41*(3), 50–68.

Collins, G. B. (1948). *Microwave [m]agnetrons* (1st ed.). New York: McGraw-Hill Book Co.

Gezahegn, Y. A., Tang, J. M., Sablani, S. S., Pedrow, P. D., Hong, Y. K., Lin, H. M., & Tang, Z. W. (2021). Dielectric properties of water relevant to microwave assisted thermal pasteurization and sterilization of packaged foods. *Innovative Food Science & Emerging Technologies, 74*.

Ghimire, A., & Chen, J. (2025). A real-time predictive complementary relative phase shifting strategy for dual-port solid-state microwave heating process. *Journal of Food Engineering, 395*, Article 112544.

Hong, Y.-K., Stanley, R., Tang, J., Bui, L., & Ghandi, A. (2021). Effect of electric field distribution on the heating uniformity of a model ready-to-eat meal in microwave-assisted thermal sterilization using the FDTD method. *Foods, 10*(2), 311.

Jain, D., Tang, J. M., Liu, F., Tang, Z. W., & Pedrow, P. D. (2018). Computational evaluation of food carrier designs to improve heating uniformity in microwave assisted thermal pasteurization. *Innovative Food Science & Emerging Technologies, 48*, 274–286.

Li, Y., Zhang, Y., Du, Y., Hong, T., Gou, D., Wang, L., & Tang, Z. (2025). A novel phase optimization method to improve microwave heating uniformity. *Journal of Food Engineering, 396*, Article 112567.

Luan, D. L., Tang, J. M., Pedrow, P. D., Liu, F., & Tang, Z. W. (2016). Analysis of electric field distribution within a microwave assisted thermal sterilization (MATS) system by computer simulation. *Journal of Food Engineering, 188*, 87–97.

Luan, D. L., Wang, Y. F., Tang, J. M., & Jain, D. (2017). Frequency distribution in domestic microwave ovens and its influence on heating pattern. *Journal of Food Science, 82*(2), 429–436.

Metaxas, A. C., & Meredith, R. J. (1993). *Industrial [m]icrowave [h]eating.* London, UK: Peter Peregrinus, Ltd.

Resurreccion, F. P., Luan, D., Tang, J., Liu, F., Tang, Z., Pedrow, P. D., & Cavalieri, R. (2015). Effect of changes in microwave frequency on heating patterns of foods in a microwave assisted thermal sterilization system. *Journal of Food Engineering, 150*, 99–105.

Ross, C., Sablani, S., & Tang, J. (2023). Preserving ready-to-eat meals using microwave technologies for future space programs. *Foods, 12*(6), 1322.

Sadiku, M. N. O. (2018). *Elements of [e]lectromagnetics* (7th ed.). New York: Oxford University Press.

Tang, J. (2015). Unlocking potentials of microwaves for food safety and quality. *Journal of Food Science, 80*(8), E1776–E1793.

Tang, J., Hong, Y.-K., Inanoglu, S., & Liu, F. (2018). Microwave pasteurization for ready-to-eat meals. *Current Opinion in Food Science, 23*, 133–141.

Tang, J., & Liu, F. (2020). *Microwave sterilization or pasteurization transport carriers.* US patent No. 10,681,923 B2.

Tang, J., Liu, F., Pathak, S. K., & Eves, I. E. E. (2006). *Apparatus and method for heating objects with microwaves.* US [P]atent [N]o. 7,119,313 B112.

Verma, K., Yang, R., Gan, H., Fathy, A., Morgan, M., & Chen, J. (2024). An integrated numerical and analytical model to understand the effect of relative phase in a dual-port solid-state microwave heating process. *Journal of Food Engineering, 367*, Article 111869.

Werner, K. (2020). The impact of solid-state RF technology on product development. In U. Erle, P. Pesheck, & M. Lorence (Eds.), *Development of [P]ackaging and [P]roducts for [u]se in [m]icrowave [o]vens* (2nd ed., pp. 415–431). Woodhead Publishing.

Yang, R., & Chen, J. (2024). Heating performance of dual-source microwave heating using different frequency shifting strategies in a solid-state system. *Food Research International, 175*, Article 113781.

Zhou, X., Czekala, P., Olszewska-Placha, M., Salski, B., Zhang, S., Pedrow, P. D., Sablani, S. S., & Tang, J. (2024). Understanding microwave heating of oils. *Journal of Food Engineering, 375*, Article 112039.

Zhou, X., Lin, H., Wu, C.-Y., Sablani, S. S., & Tang, J. (2025). A new chemical marker method for determining heating patterns in microwave pasteurization. *Journal of Food Engineering, 112593*.

Zhou, X., Pedrow, P. D., Tang, Z., Bohnet, S., Sablani, S. S., & Tang, J. (2023). Heating performance of microwave ovens powered by magnetron and solid-state generators. *Innovative Food Science & Emerging Technologies, 83*, Article 103240.

Zhou, X., & Tang, J. (2024). Microwave-[a]ssisted [t]hermal [s]terilization and [P]asteurization. In *Microwave [P]rocessing of [f]oods: Challenges, [a]dvances and [P]rospects: Microwaves and [f]ood* (pp. 253–272). Cham: Springer International Publishing.

Zhou, X., Tang, Z., Pedrow, P. D., Sablani, S. S., & Tang, J. (2023). Microwave heating based on solid-state generators: New insights into heating pattern, uniformity, and energy absorption in foods. *Journal of Food Engineering, 357*, Article 111650.